(Preprint) AAS 17-038

THE INTELLIGENT LANDING SYSTEM FOR SAFE AND PRECISE LANDING ON EUROPA

Nikolas Trawny[*], Anup Katake[†], Yang Cheng[‡], Dylan Conway[§], Miguel San Martin[¶], David Skulsky[‖], and Andrew E. Johnson[**]

Jet Propulsion Laboratory, California Institute of Technology, 4800 Oak Grove Dr., Pasadena, CA 91109

Europa, the smallest of Jupiter's Galilean moons, is thought to harbor a vast liquid water ocean beneath its icy crust, making it one of the most scientifically intriguing targets for a robotic surface sampling mission in our Solar System. However, autonomously landing a spacecraft safely and precisely on Europa poses unique challenges, such as very little existing high-resolution reconnaissance imagery, a surface expected to be very rough and hazardous over a wide range of scales, an extremely intense ionizing radiation environment, and very limited lander resources for mass and volume. To address these challenges, we propose a novel Intelligent Landing System (ILS) combining four Guidance, Navigation & Control (GN&C) sensing functions – velocimetry, altimetry, map-relative localization, and hazard detection – that would together enable safe and precise landing on Europa's surface. The ILS is a smart sensor system, combining an inertial measurement unit (IMU), a monocular, passive-optical camera, and a light detection and ranging (LiDAR) sensor with dedicated computing resources as well as an onboard 3D terrain map. The ILS leverages more than a decade of technology development from programs such as the Lander Vision System, currently baselined on the Mars 2020 mission. This paper provides a detailed description of the proposed ILS architecture and concept of operations, as well as select preliminary simulation results to assess performance and robustness.

INTRODUCTION

Thought to harbor a vast liquid water ocean beneath its icy crust, Europa is one of the Solar System's prime candidates for hosting life. As such, the science community is very interested in a lander mission, with the primary goals of searching for evidence of life on Europa, assessing its habitability in-situ, and characterizing its surface and subsurface properties at the scale of the lander to support future exploration.

A concept for such a Europa lander mission is currently being studied as a complement to NASA's planned Europa flyby mission, slated for launch in 2022. In one proposed mission design concept, the Europa lander would launch on a separate launch vehicle no earlier than 2024, and would arrive

[*]Member of Technical Staff, Guidance and Control Section, MS 198-235
[†]Member of Technical Staff, Guidance and Control Section, MS 198-235
[‡]Principal Member of Technical Staff, Mobility and Robotic Systems Section, MS 198-235
[§]Member of Technical Staff, Guidance and Control Section, MS 198-326
[¶]Engineering Fellow, Guidance and Control Section, MS 198-326
[‖]Principal Member of Technical Staff, Guidance and Control Section, MS 321-560
[**]Principal Member of Technical Staff, Guidance and Control Section, MS 198-235

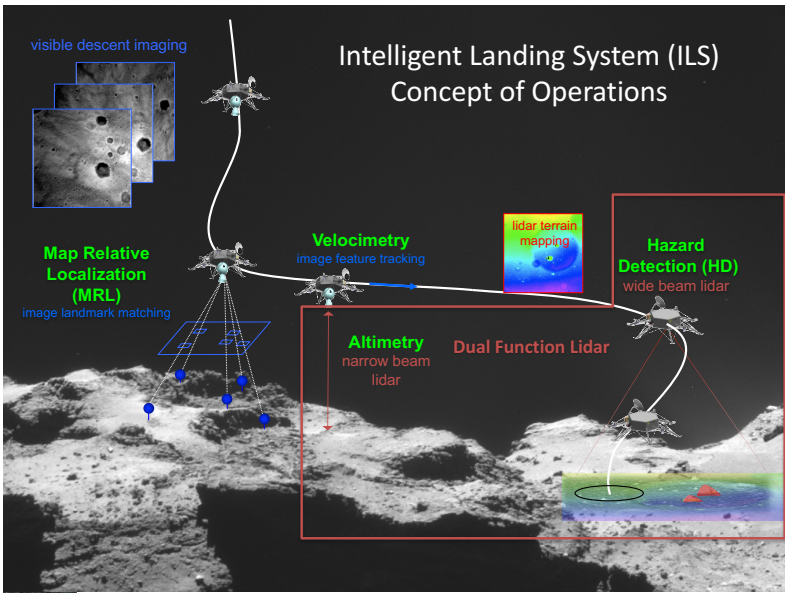

Figure 1. Artist's concept for Intelligent Landing System Guidance, Navigation & Control sensing functions.

at Jupiter after slightly less than five years of transfer time. Following separation from the carrier and orbit stage and a solid rocket motor deorbit burn, the lander would conduct a pin-point landing maneuver to touch down on the surface. However, autonomous safe and precise landing on Europa poses unique challenges. First, only very little high-resolution reconnaissance imagery is currently available of Europa's surface, reaching a maximum resolution of 6 m/pixel for a few selected sites. Based on the available data, the surface is expected to be very rough and hazardous over a wide range of scales, likely even below the best orbital images expected from NASA's planned Europa flyby mission. Second, high-energy electrons and protons trapped by Jupiter's magnetic field result in an extremely intense ionizing radiation environment, which substantially affects sensor performance, possible modes of operation, sensor component selection, and flight qualification. Finally, extremely limited lander resources for mass and volume require optimized sensor design, packaging, and shielding.

To address these challenges, we are currently designing the Intelligent Landing System (ILS), which combines four Guidance, Navigation & Control (GN&C) sensing functions – velocimetry, altimetry, map-relative localization (MRL), and hazard detection (HD) – to enable safe and precise landing on Europa's surface, as shown in Figure 1.

Safe and precise spacecraft landing is a very active area of research. A variety systems for spacecraft map-relative localization and, in some instances, velocimetry, have been proposed in the literature. Among them are APLNav,[1] developed at the Johns Hopkins Applied Physics Laboratory for lunar precision landing, the European Small Integrated Navigator for PLanetary EXploration (SINPLEX),[2] the Landstel algorithm,[3] and Draper Laboratory's Terrain-Relative Navigation & Descent Imager (TRNDI) add-on module for their GENIE Autonomous-GNC system.[4] In addition to these camera-based approaches, there also exist LiDAR-based localization techniques, e.g., based on contour matching.[5] JPL has developed the Lander Vision System (LVS),[6–9] which is currently

baselined for map-relative localization on the Mars 2020 mission and forms the basis for the ILS.

For active hazard detection, multiple sensing modalities have been proposed, including passive optical monocular camera-,[10,11] stereo camera-,[12,13] radar-,[14] and light detection and ranging (LiDAR)-based[15–17] approaches. The European Space Agency has investigated onboard HD for a variety of future lander missions.[18,19] NASA's ALHAT project demonstrated LiDAR-based HD onboard a helicopter and a terrestrial rocket vehicle.[20,21] Finally, the Chinese Chang'e-3 mission was the first to demonstrate onboard HD in an actual mission, by landing safely on the moon in December 2013.[22]

In the remainder of this paper we will first provide an overview of the ILS architecture and Concept of Operations, followed by more detail on map-relative localization, velocimetry and hazard detection. Finally, we will conclude the paper with a summary and outlook on future work.

PROPOSED ILS ARCHITECTURE

The ILS is a smart sensor system, combining an inertial measurement unit (IMU), a monocular, passive-optical camera, and a LiDAR sensor with dedicated computing resources as well as an onboard 3D terrain map, generated from prior reconnaissance data.

The IMU is shared between the GNC system and the ILS and provides spacecraft rate and specific force measurements, which are integrated to compute attitude, velocity, and position. IMU noise and biases are integrated over time, resulting in unbounded position and attitude error growth. For that reason, the ILS complements the IMU data with terrain-relative measurements of altitude from the LiDAR and position and attitude from feature matches between descent images and the onboard map, thus bootstrapping and correcting the IMU-based navigation estimate. In addition, image-to-image feature tracks, together with scale information from the LiDAR, provide six degree-of-freedom displacement measurements, which can be used to accurately estimate velocity and reduce the position error growth rate. The current design of the ILS camera envisions a 1024×1024 pixel, greyscale CMOS imager with 60° field of view, with appropriate shielding for the Europan radiation environment and fast optics to limit motion blur and radiation flux effects.

The dual mode LiDAR will provide both dense 3D mapping at 500 m altitude for HD, as well as low update rate altimetry starting at 8 km altitude down to 10 m altitude. The required extent and resolution of the 3D map will likely necessitate a scanning mechanism. To our knowledge, an off-the-shelf, space-qualified LiDAR for the requirements of a Europa Lander currently does not exist, and therefore the LiDAR sensor is currently the focus of intense technology development efforts. More details are described in the section on Hazard Detection.

Image and map processing are computationally intensive and therefore require dedicated computing resources. The ILS software is being designed to run on a general purpose BAE RAD-750 flight processor, and two dedicated computer vision accelerator cards (CVAC) currently being built for LVS, consisting of a Virtex-5 FPGA, a "housekeeping" FPGA, rad-hard volatile and non-volatile memory banks and various sensor and testing I/O interfaces. One CVAC will be handling the camera image processing, while the second is dedicated to HD. The CVAC will undergo minor redesign to accommodate the radiation exposure inside the avionics vault.

PROPOSED ILS CONCEPT OF OPERATIONS

In the notional timeline, approximately 2.5 h before landing, the Lander Deorbit Vehicle (DOV) separates from its Carrier, marking the beginning of the Deorbit, Descent, and Landing (DDL)

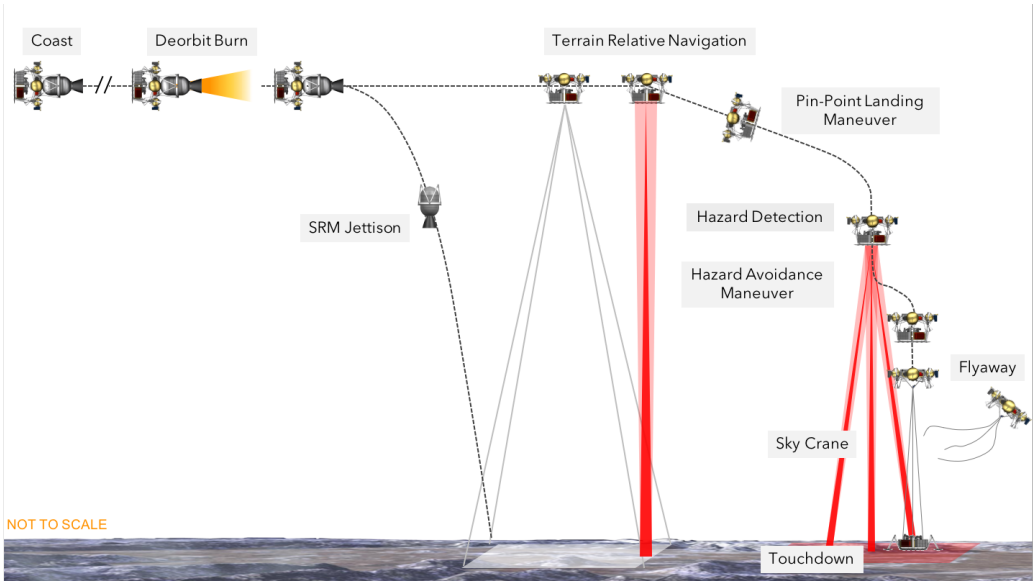

Figure 2. ILS operation during the Deorbit, Descent, and Landing Phase of the Europa Lander concept.

Phase, which ends shortly after touchdown (see Figure 2). About 5 minutes before touchdown, a solid rocket motor (SRM) decelerates the DOV from 1950 m/s to 100 m/s at an altitude of 5 km. After SRM burnout and jettison, the vehicle will slew to nadir-pointing attitude, and the ILS will start acquiring images and LiDAR measurements. A first MRL position estimate approximately 10s after start of ILS operations will be used to initiate the Pin-Point Landing (PPL) maneuver. The objective of this maneuver is to steer the powered descent vehicle (PDV) to a position vertically above the target landing site, at an altitude of 1000 m with zero horizontal and -30 m/s vertical velocity. A second MRL update may happen for fine positioning once the PDV is over the area near the target landing site for which high-resolution maps are available. HD will begin at an altitude of 500 m, when the LiDAR will create a 100 m $\times$100 m elevation map of the landing area and process it to construct a landing safety map and select a safe landing site. This process is designed to complete in 3 s. A hazard avoidance maneuver will then start at 250 m altitude and guide the PDV to a point 30 m above the selected safe landing site, with a vertical velocity of -0.5 m/s. At an altitude of 21 m, the Lander separates from the Descent Stage and is lowered on a 10 m bridle to the ground. Once touchdown is detected, the bridle is cut and the Descent Stage performs a Fly Away maneuver. Image-to-image feature tracking and LiDAR altimetry will be used for velocimetry and altimetry from SRM jettison to touchdown.

MAP-RELATIVE LOCALIZATION

Map-relative localization currently follows the LVS design, where localization is divided into a coarse and a fine match phase. The coarse match phase uses five large templates per image for three images and searches for a match in the entire surface reflectance map (SRM) using FFT-based correlation. The 3D position coordinates of the matched feature are then computed by querying the SRM and DEM at the location of the interpolated subpixel location of the correlation peak. The spacecraft horizontal position is then estimated in a batch least squares estimator. The coarse phase is designed to robustly estimate a large, 2 km initial horizontal position error. It is followed by a

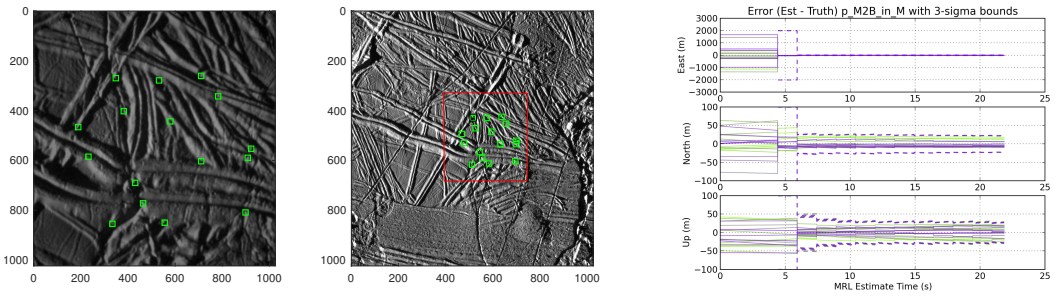

(a) Example descent image (left) and Europa map (right), with image footprint marked in red and feature matches shown as green squares.

(b) MRL position error in East-North-Up frame and associated 3-sigma bounds.

Figure 3. Preliminary simulation results for a nominal lander trajectory at 5 km altitude with 2 km downtrack initial knowledge error indicate that localization performance on order of 50 m per axis appears feasible during the first MRL solution phase after SRM burn-out.

fine localization phase, during which a large number of features with smaller feature template size are matched over a smaller search window region using normalized spatial cross correlation, thus trading robustness and map coverage for accuracy. In this phase, the spacecraft state is estimated using an extended Kalman filter. The map-relative localization process, including a variety of internal consistency checks, takes approximately 10 s.

The current FPGA image processing firmware is designed for 1024×1024 pixel maps. The raw map should be sized to fully contain the image footprint for the entire 10 s of operations. This includes delivery error, knowledge error, ground track during LVS operation, off-nadir angle excursions, as well as margin. In addition, the image footprint is a function of spacecraft trajectory and camera field of view. At the beginning of MRL, the delivery error induced by SRM burn variations will be known, and a smaller coarse map can be cropped from the raw map. Dividing the required coarse map extent by the number of pixels yields the highest useful resolution for the coarse map. For a 60° field of view camera, at 5 km altitude, the coarse map should cover at least 14 km, with a highest useable resolution of 14 m/pixel, which is in line with the expected capability of the Europa fly-by mission wide-angle camera. Map quality will be of paramount importance for matching accuracy. Particularly significant is the difference in lighting conditions between map and descent images. The lack of atmosphere results in sharp shadows, whose changing shape and direction over the course of a Europan day can significantly degrade matching performance if they differ too much from those present in the map. Initial studies indicate a sharp drop off in matching performance after a discrepancy between map and descent image lighting conditions in excess of 25° sun elevation angle. Fortunately, since the time of landing will be known well in advance, the onboard map can be rendered on the ground to reflect the expected lighting conditions. The impact of errors in the reconnaissance elevation data on the rendered MRL map is subject of ongoing study.

Initial simulation results using the LVS simulator (LVSS) and a scaled map generated from Galileo imagery[23] shown in Figure 3 indicate that with a 16 m/pixel map and nominal IMU and image matching errors, position accuracy on order of 50 m per axis should be achievable during the first MRL solution phase after SRM burn-out. Note that these simulations do not yet include all error sources, e.g., lighting differences between descent image and map, map errors, or radiation artifacts.

VELOCIMETRY

In addition to image-to-map feature matching, the ILS will also perform image-to-image feature tracking. This capability does not require an onboard map, and – unlike MRL, which will fail once the difference between image and map resolution exceeds a threshold – can work over the entire range of DDL altitudes. Image-to-image feature tracking, together with scale information from the LiDAR, provides a six degree-of-freedom delta-position and delta-attitude measurement between consecutive images. This measurement provides information about spacecraft velocity (hence its use for velocimetry) and limits the growth rate of attitude and position drift. The velocity accuracy increases with decreasing altitude. Accurate velocity knowledge is of critical importance for lander guidance and control, particularly in the final sky-crane phase of DDL. The current ILS estimation framework for velocimetry is based on the Minimal State Augmentation Algorithm for Vision-Based Navigation (MAVeN) developed at JPL. Unlike Simultaneous Localization and Mapping (SLAM), MAVeN is estimating the camera position of certain keyframes rather than the 3D positions of surface features, resulting in a robust and computationally inexpensive algorithm. It is relying on several key assumptions: (a) availability of faceted shape model of Europa (which can be constructed from the DEM), (b) knowledge of spacecraft attitude (which is justifiable in the Europa lander GNC design including precise star tracker attitude initialization and space-grade IMU gyroscopes), and (c) availability of a camera, LiDAR altimeter and IMU (which is precisely the sensor suite of the ILS).

MAVeN works as follows. Images taken by the camera are broken into sequences that start by taking a base image, followed by several search images. Once the number of successful feature matches between a search image and the base image falls below a threshold, a new base image is taken and the process repeats. For each base image, interest points are found and used to create pseudo-landmarks for use by subsequent search images. Specifically, pseudo-landmarks are created by projecting the measured bearing directions for each interest point seen in the base image down onto a facet model of the Europan surface. The resulting feature locations on the facet model serve as pseudo-landmarks that are processed in subsequent search images as if they were real landmarks, i.e., as if they were known a-priori mapped locations on the surface. Their position error and the ensuing correlations are captured in the state estimator formulation by adding the spacecraft position estimate at the time the base image was acquired to the state vector.

The image processing required for image-to-image feature tracking is similar to that for MRL and was implemented on the LVS prototype. Results from a helicopter field test in the Mojave desert shown in Figure 4 demonstrate excellent tracking performance.

HAZARD DETECTION

Active hazard detection and avoidance is considered as an essential element for safe landing on Europa. As compared to landing on Mars, for which high resolution digital elevation model (DEM) data is available through prior missions and imagery obtained from existing orbital assets, there exists no such data or assets at Europa. While Europa Clipper may provide high resolution images of potential landing sites, their availability or coverage or resolution cannot be guaranteed nor assumed. The use of MRL helps to avoid large scale hazards in the landing ellipse that can be identified in reconnaissance imagery, but not at scales that are equivalent to the lander footprint or tolerance to hazards.

Figure 5 illustrates a notional timeline for the hazard detection (HD) sub-phase of DDL. At ap-

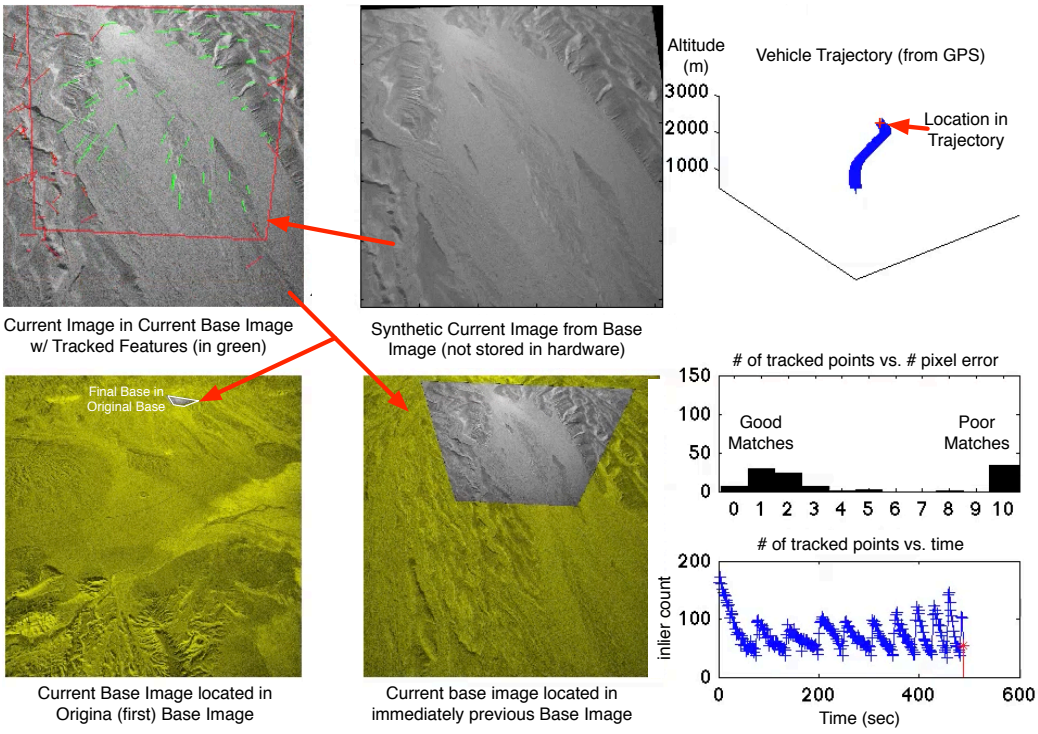

Figure 4. Image-to-image feature tracking results during helicopter field test in Mojave desert.

proximately 1 km altitude, the lander performs maneuvers to align and position itself over the center of the target landing site. Following this, the lander performs a powered descent by firing its thrusters to maintain a 30 m/s vertical descent rate. At 500 m altitude, the 3D mapping of the landing site is initiated. Given the fuel constraints and timeline of operations, the maximum divert distance that the lander can perform to avoid hazards is on the order of 40 m in radius. A 10 m margin on the divert distance implies that the landing area under consideration is 50 m in radius or equivalently 100 m $\times$ 100 m. On-board HD processing algorithms will evaluate the acquired LiDAR data to identify and target a safe site of size 5 m in diameter. This is done by computing the slope and roughness maps over the scale of the lander, combining these two to create a safety map based upon a required cost function and subsequently selecting a safe site with the lowest cost.[24]

From a point of view of the sensing performance needs - the lander spacecraft is approximately 2 m in diameter and will land on the surface using a legged mechanism. The landing feet are approximately $15 - 20$ cm in size, and it is required that they do not land on hazards equivalent in size. A minimum of $3 - 4$ 3D pixels are required over this footprint, which results in requiring a 5 cm per pixel of ground sample distance. This implies that the resultant 3D map which covers the 100 m $\times$ 100 m area is at a minimum 2000×2000 pixels in size. The legged lander is also sensitive to hazards that are 15 cm tall. The chaotic nature of Europa's terrain could contain hazards that are limited to a few 10s of centimeters in horizontal extent while being large in the vertical, akin to stalagmites or penitentes[25] as seen on Earth. Therefore, a 3D range measurement error of 5 cm (3σ) is required to detect such hazards with high reliability.

Approximately 3 seconds have been allotted for performing the data collection, mapping, detecting hazards and selecting a safe site for landing. A notional subdivision of these 3 seconds is as

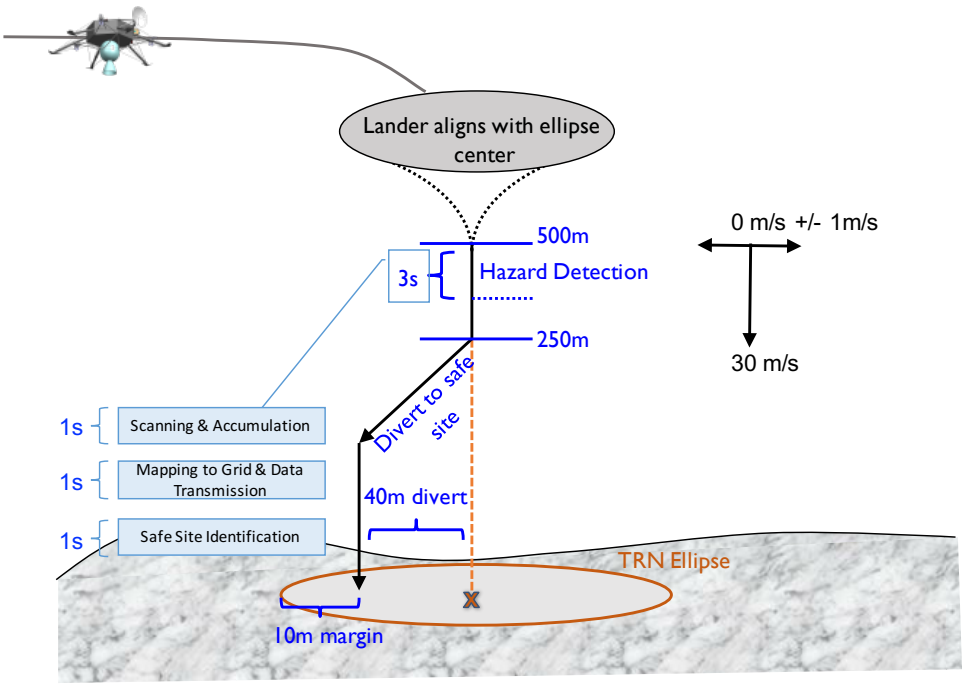

Figure 5. Timeline and concept of operations for the hazard detection sub-phase

follows:

- 1 second: for acquiring the 3D data over the 100 m $\times$ 100 m landing site
- 1 second: for mapping the acquired data to a grid and transmission of this data to the HD data processor located in the spacecraft GN&C avionics sub-system
- 1 second: for the HD data processor to evaluate the 3D map, detect hazards and select a safe landing site

Lidar based Sensing

A LiDAR that can be deployed in the DDL phase for Europa faces significant design challenges. Firstly, the requirement to acquire a 3D range data over a 100 m $\times$ 100 m area at better than 5 cm ground sample distance in less than 1 second implies a LiDAR that is capable of throughput which is better than 4 million valid samples/s. To the best of our knowledge, such a LiDAR does not exist as of today. While there are LiDAR solutions, primarily operating in the modalities of single photon detection or Geiger mode, that are capable of acquiring range samples at such rates, the data acquired must be heavily filtered using probabilistic algorithms to remove noise and arrive at a valid set of measurements. Such processing is typically done off-line using high performance graphics processing units and can take multiple hours to result in a digital elevation map that can be ultimately used. Such processing luxury however is not available for the resource constrained Europa lander. Lidars operating in the linear mode regime do not need such noise filtering, however, they are limited by the data acquisition rates which are typically around $10 - 100$ kHz. Flash mode LiDARs such as those from Advanced Scientific Concepts[26] and Ball Aerospace[27] require a large number of photons

to be able to register a valid return pulse, and therefore are limited in the acquisition by laser pulse energies, pulse repetition rates, and signal sampling rates.

Another challenge for the Europa LiDAR is that the LiDAR must also be capable of dual mode operation wherein it not only provides dense 3D mapping at 500 m altitude, but also provides low update rate altimetry starting at 8 km altitude down to 10 m altitude. This multiple orders of magnitude variation in operational range requires a sensor of large dynamic range that is difficult to achieve using a single laser/detector combination. Typically, a combination of high and low pulse energy laser is used to address this issue in scanning LiDARs or a beam diffuser is employed in the electro-optical path for flash LiDARs. A dual laser solution is not attractive from a point of view of mass and volume, while the beam diffuser presents an added risk with regards to moving parts.

Lastly, and perhaps most importantly, the LiDAR sensor system and its associated processing electronics must be compact and light-weight. Landing on the Europan surface requires a very large mass penalty - i.e. for every kilogram of landed surface payload, a $50\times$ launch mass is required. Thus, the LiDAR must be mass, power and volume efficient. This implies that major components of the LiDAR such as the laser, detector and scanning (if required) must be designed from a systems perspective and in close harmony with each other. As an example - it is our belief that reducing the laser pulse energies leads to a series of highly beneficial and coherent impacts on other components that potentially will enable meeting the performance as well as result in a low size, weight, and power (SWAP) sensor system.

Considerations for 3D Map Creation

While a 2000×2000 pixel focal plane array coupled with an equivalent laser assembly would provide the required coverage instantaneously, it might lead to an infeasible architecture or result in a system configuration that is high in SWAP. Therefore, a scanning based approach is most likely need to provide the required coverage. In this approach a 2D array of pixels (eg. 256×256, 1024×8 etc.) could be rapidly scanned across the field of regard using two-axis scan mechanisms such as fast steering mirrors or dual-wedge scanners. However, proper attention must be paid when using a scan assembly while creating a 3D map. Specifically, vehicle motion during the scan, and subsequently the use of stitching algorithms to seamlessly assemble the large area map from individual frames or maplets are the two biggest concerns. Vehicle motion during scans can result in discontinuities in coverage, range artifacts along scan seams, non-uniform sampling density as well as variable maplet footprints (e.g., zoom effect with decreasing altitude). Thus it is critical to understand the detector-scanner interplay and arrive at an architecture that mitigates the concerns and issues associated with a scanning system.

Challenges of the Environment at Europa

Even if we were to imagine for a moment that a LiDAR capable of meeting the high performance requirements is readily available, the extreme environment at Europa presents a daunting challenge with regards to sensor design and use. Due to its proximity to Jupiter, Europa resides in a severe radiation zone with a very high concentration of trapped energetic particles. Initial analyses on nominal trajectories for landing on Europa show an accumulated total ionizing dose of 1.3 Mrad behind 100 mil of aluminum shielding and radiation design factor of $1\times$, with majority of it being accumulated towards the end of the mission. For electro-optical components such as the detector array, displacement damage dose (DDD) is a major contributor to defect creation and therefore

increased noise in semiconductors. The components are expected to see a DDD of 3.2×10^9 MeV/g-Si over the mission duration which is orders of magnitude more severe than that of typical missions. This implies that the components chosen for the sensors must be radiation hardened by design to the greatest extent possible, and in addition be shielded using a combination of spot and global shields with appropriate materials. The need for extensive shielding now results in a significant addition of mass and volume to the sensor assembly, further exacerbating the SWAP concerns.

Besides accumulated dose, one must also be very concerned of flux (#/cm^2-s) effects on the sensor measurements during acquisition. Since a particle hitting the detector assembly deposits large amounts of charge along its path, this can easily overwhelm the received useful signal of the laser pulse. This could be especially problematic in detectors that are based upon single photon or Geiger mode detection, wherein a distinction cannot be made between a photoelectron from a laser pulse return or a radiation hit or background dark noise. While shielding will reduce the particle flux, depending upon the materials used, this could also result in generation of secondary particles that would behave analogous to the primary ones and corrupt the measurements. Thus a very careful and rigorous analysis and design of optimal shielding is critical.

Due to its potential to harbor life in its oceans, missions to Europa must undergo very stringent planetary protection requirements to reduce bioburden as much as possible. This then immediately applies to the sensor systems that the lander carries. The two proposed techniques for reducing micro-organisms burden - high temperature bake-out over extended duration and immersion in hydrogen peroxide, are not amenable to use on surfaces of electro-optical components which are usually very temperature and abrasion sensitive. Thus robust sensor designs must be developed to address planetary protection concerns.

CONCLUSION

The ILS as described in this paper would form a critical component of the navigation sensor suite of the proposed Europa Lander mission concept. The combination of four core capabilities necessary for safe and precise landing – map-relative localization, velocimetry, altimetry, and hazard detection – is significantly advancing the state of the art for space-qualified GNC sensors, and is considered enabling technology for a safe landing on a moon as hazardous as Europa.

The ILS technology would also enable new science for other future missions that land on planets, icy moons, asteroids or comets, by allowing to touch down near sites of maximum science value while actively detecting and avoiding landing hazards. In addition, camera-based velocimetry constitutes a compact alternative to doppler-based RF or LiDAR velocimetry sensors.

As discussed, the various challenges facing a Europa lander – radiation, limited knowledge of surface properties and topology at lander scale, and severe mass and volume constraints, to name a few – will require a significant amount of careful and rigorous design and analysis. Particular efforts are made in the area of algorithm robustness against radiation artifacts, lighting condition differences, errors in albedo and elevation maps, and terrain effects. In addition, significant investments are made in hardware development, particularly for the LiDAR, to meet performance, address planetary protection requirements, and survive the harsh Europan environment.

ACKNOWLEDGMENTS

This research was carried out at the Jet Propulsion Laboratory, California Institute of Technology, under a contract with the National Aeronautics and Space Administration.

REFERENCES

[1] T. G. McGee, P. E. Rosendall, A. Hill, W. J. Shyong, T. B. Criss, C. Reed, G. Chavers, M. Hannan, C. Epp, and M. Nishant, "APLNav: Development Status of an Onboard Passive Optical Terrain Relative Navigation System," *Proc. AIAA Guidance, Navigation, and Control Conference*, Kissimmee, FL, Jan. 05–09, 2015, doi:10.2514/6.2015-0853.

[2] S. Steffes, M. Dumke, D. Heise, M. Sagliano, M. Samaan, S. Theil, E. Boslooper, H. Oosterling, J. Schulte, D. Skaborn, S. Söderholm, S. Conticello, M. Esposito, Y. Yanson, B. Monna, F. Stelwagen, and R. Visee, "Target relative navigation results from hardware-in-the-loop tests using the SINPLEX navigation system," *Proc. 37th Annual AAS Guidance and Control Conference*, No. AAS 14-402, Breckenridge, CO, Feb. 2014.

[3] B. Van Pham, S. Lacroix, and M. Devy, "Vision-based Absolute Navigation for Descent and Landing," *J. Field Robot.*, Vol. 29, July 2012, pp. 627–647, 10.1002/rob.21406.

[4] T. Steiner and T. Brady, "Vision-based navigation and hazard detection for terrestrial rocket approach and landing," *Proc. IEEE Aerospace Conference*, Mar. 2014, pp. 1–8, 10.1109/AERO.2014.6836216.

[5] A. Johnson and T. Ivanov, "Analysis and Testing of a LIDAR-Based Approach to Terrain Relative Navigation for Precise Lunar Landing," *Proc. AIAA Guidance, Navigation, and Control Conference*, Aug. 2011, doi:10.2514/6.2011-6578.

[6] J. Montgomery, Y. Cheng, A. Katake, N. Trawny, B. Tweddle, J. Zheng, and A. Johnson, "The Mars 2020 Lander Vision System," *Proc. International Planetary Probe Workshop*, Laurel, MD, July 13-17, 2016.

[7] A. E. Johnson, Y. Cheng, J. F. Montgomery, N. Trawny, B. Tweddle, and J. X. Zheng, "Real-Time Terrain Relative Navigation Test Results from a Relevant Environment for Mars Landing," *Proc. AIAA Guidance, Navigation, and Control Conference*, Kissimmee, FL, Jan. 05 - 09, 2015, doi:10.2514/6.2015-0851.

[8] A. E. Johnson, Y. Cheng, J. Montgomery, N. Trawny, B. E. Tweddle, and J. Zheng, "Design and Analysis of Map Relative Localization for Access to Hazardous Landing Sites on Mars," *Proc. AIAA Guidance, Navigation, and Control Conference*, San Diego, CA, Jan. 21, 2016, doi:10.2514/6.2016-0379.

[9] N. Trawny, J. Benito, B. Tweddle, C. F. Bergh, G. Khanoyan, G. M. Vaughan, J. X. Zheng, C. Y. Villalpando, Y. Cheng, D. P. Scharf, C. D. Fisher, P. M. Sulzen, J. F. Montgomery, A. E. Johnson, M. Aung, M. W. Regehr, D. Dueri, B. Açikmeşe, D. Masten, T. O'Neal, and S. Nietfeld, "Flight testing of terrain-relative navigation and large-divert guidance on a VTVL rocket," *Proc. AIAA SPACE 2015 Conference and Exposition*, Pasadena, CA, Aug. 2015.

[10] E. S. Crane, *Vision-based hazard estimation during autonomous lunar landing*. PhD thesis, Stanford University, Stanford, CA, June 2014.

[11] A. Huertas, Y. Cheng, and R. Madison, "Passive imaging based multi-cue hazard detection for spacecraft safe landing," *2006 IEEE Aerospace Conference*, 2006, pp. 1–14, 10.1109/AERO.2006.1655794.

[12] L. Matthies, A. Huertas, Y. Cheng, and A. Johnson, "Stereo vision and shadow analysis for landing hazard detection," *IEEE International Conference on Robotics and Automation (ICRA)*, May 2008, pp. 2735–2742, 10.1109/ROBOT.2008.4543625.

[13] S. Woicke and E. Mooij, "Passive Hazard Detection for Planetary Landing," *AIAA Guidance, Navigation, and Control Conference*, American Institute of Aeronautics and Astronautics, Jan. 4–8, 2016, doi:10.2514/6.2016-1133.

[14] B. D. Pollard, G. Sadowy, D. Moller, and E. Rodriguez, "A millimeter-wave phased array radar for hazard detection and avoidance on planetary landers," *Proc. 2003 IEEE Aerospace Conference*, Vol. 2, March 2003, pp. 1115–1122, 10.1109/AERO.2003.1235525.

[15] S. Chakroborty, O. Aboutalib, and C. Meade, "Autonomous Lunar Lander Hazard Detection and Avoidance System," *AIAA SPACE 2009 Conference & Exposition*, American Institute of Aeronautics and Astronautics, Sept. 14–17, 2009, doi:10.2514/6.2009-6452.

[16] J. de Lafontaine, D. Neveu, and K. Lebel, "Autonomous Planetary Landing Using a LIDAR Sensor: the Closed-Loop System," *Guidance, Navigation and Control Systems*, Vol. 606 of *ESA Special Publication*, Jan. 2006.

[17] R. Frampton, J. Ball, K. Oittinen, S. Tandon, D. Schwab, M. Bishun, B. Richards, and J. Tripp, "GN&C, and Precision Landing and Hazard Avoidance Technology Demonstration," *AIAA SPACE 2007 Conference & Exposition*, American Institute of Aeronautics and Astronautics, Sept. 18–20, 2007, doi:10.2514/6.2007-6174.

[18] F. M. Kolb, I. Ahrns, and B. Moebius, "3D Imaging LIDAR for Autonomous Planetary Landing," *Proc. i-SAIRAS*, Sapporo, Japan, Aug. 29 – Sept. 1, 2010, pp. 152–156.

[19] B. Parreira, J. Vasconcelos, J. Montaño, J. Ramón, and L. F. Penin, "Hazard Detection and Avoidance in ESA Lunar Lander: Concept and Performance," *AIAA Guidance, Navigation, and Control (GNC) Conference*, Boston, MA, American Institute of Aeronautics and Astronautics, Aug. 19–22, 2013, doi:10.2514/6.2013-5020.

[20] N. Trawny, J. M. Carson, A. Huertas, M. E. Luna, V. E. Roback, A. E. Johnson, K. E. Martin, and C. Y. Villalpando, "Helicopter Flight Testing of a Real-Time Hazard Detection System for Safe Lunar Landing," *AIAA SPACE 2013 Conference and Exposition*, San Diego, CA, American Institute of Aeronautics and Astronautics, Sept. 10–12, 2013, doi:10.2514/6.2013-5313.

[21] N. Trawny, A. Huertas, M. E. Luna, C. Y. Villalpando, K. Martin, J. M. Carson, A. E. Johnson, C. Restrepo, and V. E. Roback, "Flight testing a Real-Time Hazard Detection System for Safe Lunar Landing on the Rocket-Powered Morpheus Vehicle," *AIAA Guidance, Navigation, and Control Conference*, Kissimmee, FL, American Institute of Aeronautics and Astronautics, Jan. 5–9, 2015, doi:10.2514/6.2015-0326.

[22] X. Jiang, S. Li, and T. Tao, "Innovative hazard detection and avoidance strategy for autonomous safe planetary landing," *Acta Astronautica*, Vol. 126, 2016, pp. 66 – 76, http://dx.doi.org/10.1016/j.actaastro.2016.02.028.

[23] P. Schenk, *Atlas of the Galilean Satellites*. Cambridge University Press, 2010.

[24] M. E. Luna, E. Almeida, G. Spiers, C. Y. Villalpando, A. E. Johnson, and N. Trawny, "Evaluation of the Simple Safe Site Selection (S4) Hazard Detection Algorithm using Helicopter Field Test Data," *AIAA Guidance, Navigation, and Control Conference*, 2017, p. 1497.

[25] D. Hobley, J. Moore, and A. Howard, "How Rough is the Surface of Europa at Lander Scale?," *Lunar and Planetary Science Conference*, Vol. 44, 2013, p. 2432.

[26] R. Stettner, "Compact 3D flash lidar video cameras and applications," *SPIE Defense, Security, and Sensing*, International Society for Optics and Photonics, 2010, pp. 768405–768405.

[27] R. Rohrschneider, C. Weimer, J. Masciarelli, M. Lieber, C. Adkins, and J. Domber, "Vision Navigation Sensor (VNS) with Adaptive Electronically Steerable Flash LIDAR (ESFL)," *AIAA Guidance, Navigation, and Control Conference*, 2016, p. 2096.

